
Article:
Naydenov, Genadi, Hasnip, Philip orcid.org/0000-0002-4314-4093, Lazarov, Vlado orcid.org/0000-0002-4314-6865 et al. (1 more author) (2019) Effective modelling of the Seebeck coefficient of Fe2VAl. Journal of physics : Condensed matter. 125401. ISSN 1361-648X

https://doi.org/10.1088/1361-648X/ab5867

Effective modelling of the Seebeck coefficient of Fe₂VAl

Effective modelling of the Seebeck coefficient of Fe_2VAl

G A Naydenov, P J Hasnip, V K Lazarov and M I J Probert

Department of Physics, University of York, York YO10 5DD, United Kingdom

E-mail: gan503@york.ac.uk

July 2019

Abstract. Previous first-principles calculations have failed to reproduce many of the key thermoelectric features of Fe_2VAl, e.g. the maximum values of the Seebeck coefficient S and its asymmetry with respect to the chemical potential. Also, previous theoretical predictions suggested that the pseudo band gap of Fe_2VAl switches from indirect to direct upon doping. In this work, we report first-principles calculations that correctly reproduce the experimentally measured thermoelectric properties of Fe_2VAl. This is achieved by adding a larger Hubbard U term to V atoms than to Fe atoms and including a scissors operator afterwards. As a result, bulk Fe_2VAl is modelled as a gapless semiconductor with maximum S values of 76 and -158 μV/K for p- and n-type, respectively, which agree well with the experimental measurements.

1. Introduction

Fe_2VAl is a Heusler-type intermetallic compound which has been extensively studied as a potential thermoelectric material due to its ecologically friendly properties and earth abundance of Fe, V and Al [1, 2, 3, 4]. Fe_2VAl alloys have a very large power factor comparable to some of the best thermoelectrics, e.g. Bi_2Te_3. However, their thermal conductivity, which is about 10 times higher than Bi_2Te_3, results in a small thermoelectric figure of merit (ZT) [5, 6]. The high thermal conductivity of Fe_2VAl is phonon dominated and provides much room for improvement of ZT, hence several theoretical and experimental studies which aim to optimise the thermal conductivity (κ) as well as the Seebeck coefficient (S) and electrical conductivity (σ) have been conducted in the past two decades [2, 3, 7, 8, 9, 10, 11, 12].

The majority of the thermoelectric properties can be calculated from the density of states (DOS), the conductivity tensor and the group velocity of the electrons [13]. Therefore, it is important to obtain a proper electronic structure in order to calculate the transport properties correctly. In the case of Fe_2VAl, bulk band structure calculations [7, 14, 15, 16, 17, 18, 19, 20] consistently predict the presence of an *indirect* pseudo band gap at the Fermi level. In contrast to these predictions, experimental measurements of Fe_2VAl alloys show typical behaviour for *direct* band

gap semiconductors with hole carriers. Photoelectronic spectroscopy [1, 21] and optical conductivity measurements [22] confirm the existence of a pseudo band gap without taking into account the **k**-dependence and hence cannot distinguish between direct and indirect gaps. These studies show that the widely accepted and theoretically predicted level of E_F in the band structure of Fe_2VAl cannot explain both the experimentally measured hole carrier concentration [23] and the lack of temperature dependence in optical conductivity [22]. Moreover, recent Angle-resolved photoemission spectroscopy (ARPES) measurements of off-stoichiometric Fe_2VAl alloys mapped the **k**-dependence and showed that no conduction bands are crossing the Fermi level at the high symmetry X-point in the irreducible Brillouin zone [24], once again disagreeing with the theoretically predicted band structure [16, 17, 18, 20, 25, 26].

In addition, current theoretical band modelling underestimates the maximum value of the Seebeck coefficient (S) and cannot explain its asymmetry with respect to doping [7]. Several studies have tried to explain the magnitude of S (for both n- and p-type doping) by modifying the electron-electron exchange-correlation functional [16, 17], by including the Hubbard U [18] or by considering the effect of anti-site defects [12, 16]. In all cases the calculations failed to model the asymmetric behaviour of the Seebeck coefficient and thus overestimated the maximum value of S for p-type doping. In this work, we use a very pragmatic approach to the problem and show that conduction bands responsible for the p-type behaviour of Fe_2VAl come from Fe rather than V, and as a result the experimentally measured values of the Seebeck coefficient can be reproduced, but only if a larger Hubbard U term is added to V than to Fe. We also thoroughly investigate the band structure of Fe_2VAl, describe how the bands fold when the size of the simulation cell is changed and show that the periodicity of the conduction bands is changed by the inclusion of the Hubbard U. Also, the Hubbard U model can predict the asymmetry in the Seebeck coefficient, i.e. the dependence of S on the chemical potential.

2. Calculations setup

2.1. Crystal structure of Fe_2VAl

Heusler alloys have chemical formula X_2YZ, where X and Y are transition metals and Z is a main group element. Calculations were performed on the ordered $L2_1$ structure of Fe_2VAl, which is shown in Fig. 1. The structure is face-centred cubic, having space group $Fm\bar{3}m$ (225). There are four Fe_2VAl formula units (f.u.) in the cubic unit cell. A primitive rhombohedral unit cell, which contains 1 f.u., can be extracted from the cubic cell. The Fe atoms in the rhombohedral cell have fractional coordinates of (1/4, 1/4, 1/4) and (3/4, 3/4, 3/4), while Al are at (1/2, 1/2, 1/2) and V are at (0, 0, 0). Bulk properties of Heusler alloys are usually calculated with a primitive unit cell, whereas doped systems are investigated with a supercell in order to obtain the desired doping concentration.

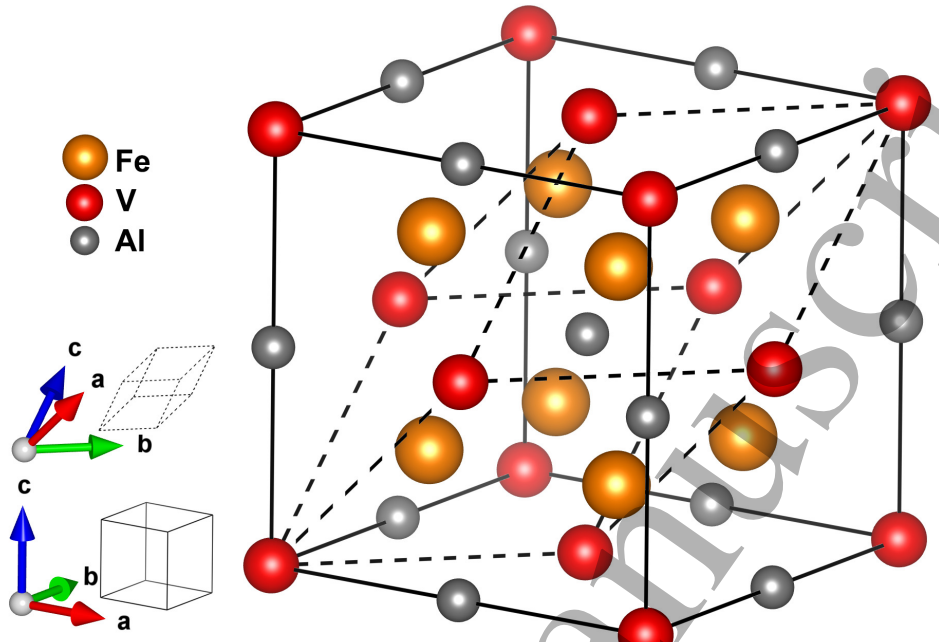

Figure 1. Schematic of the cubic (solid lines) and rhombohedral (dashed lines) Fe_2VAl unit cell. Fe atoms (orange) reside at (1/4, 1/4, 1/4) and (3/4, 3/4, 3/4), Al (grey) at (1/2, 1/2, 1/2) and V (red) at (0, 0, 0).

2.2. Density functional theory calculations settings

The first principles calculations were performed with the CASTEP [27] code and a GGA-PBE exchange-correlation functional [28]. On-the-fly ultrasoft pseudopotentials (C9 set) were used with a plane-wave cut-off energy of 700 eV with a grid scale of size 2.0. The Brillouin zone was sampled using a Monkhorst-Pack [29] grid with a $24 \times 24 \times 24$ **k**-points mesh (equivalent to **k**-points spacing of 0.013 2πÅ^{-1}) for the rhombohedral unit cell. Spin-orbit coupling was included for the rhombohedral cells but did not influence the final results significantly and therefore was not considered for the other cases. The structure was fully optimized until pressure and energy were converged to 0.01 GPa and 0.02 meV/atom, respectively. Transport properties were calculated using the semi-classical Boltzmann transport formalism within the constant relaxation time approximation as implemented in the BoltzTraP code [13]. BoltzTraP calculates both electrical and electron thermal conductivity as σ/τ and κ_{el}/τ where τ is the relaxation time and is obtained by fitting to experimental results. The eigenenergies required for the transport properties were calculated with a $48 \times 48 \times 48$ **k**-points mesh. Density of states (DOS) and partial density of states (PDOS) were analysed using the OptaDOS code [30].

2.3. Theoretical expectations

Theoretically, the relation between the thermoelectric figure of merit, ZT, and S, σ, and κ, is given by Eqn. 1:

$$ZT = \frac{S^2 \sigma T}{\kappa}, \tag{1}$$

where σ and κ are the electrical and thermal conductivity, respectively.

One of the requirements for a good thermoelectric material is the presence of a rapid change in the density of states across the Fermi level (E_{F}). This can be explained with the formula for the Seebeck coefficient S (T) for metallic systems at a given temperature T [31]:

$$S(T) = \frac{\pi^2 {k_{\mathrm{B}}}^2 T}{3(-e)} \Big(\frac{\partial \ln \sigma(E)}{\partial E} \Big)_{E=E_F}. \tag{2}$$

Considering that the electrical conductivity $\sigma(E)$ is proportional to the density of states, $N(E)$, it could be shown with Eqn. 2 that a steep slope, $\partial N(E)/\partial E$, near E_{F}, would result in a large Seebeck coefficient and better ZT. Thus, semiconductors whose DOS varies rapidly on either side of the band gap are considered as promising candidates for efficient new thermoelectric materials. The purpose of Eqn. 2 is to highlight this point, whereas the actual Seebeck coefficient is computed in accordance with the BoltzTraP implementation.

3. Electronic structure

We start by presenting the electronic properties and band structure of Fe_2VAl using a primitive rhombohedral cell without the inclusion of the Hubbard U on any of the atoms. After relaxation, the optimized lattice constant of the primitive rhombohedral cell was found to be 4.03 Å (equivalent to 5.70 Å for a cubic cell). The obtained lattice constant is smaller than the experimental value of 5.76 Å [1, 26] by 1%, similar to other *ab initio* GGA-PBE studies [7, 14, 25]. Spin-polarised calculations showed that Fe_2VAl is nonmagnetic, in good agreement with other theoretical [21, 32, 10] and experimental [1, 14] studies.

Fig. 2(a) and (b) show the band structure of Fe_2VAl in the irreducible Brillouin zone and the contribution of the V and Fe d-orbitals to the total DOS near E_{F}, respectively. Fig. 2(a) shows the small overlap between the bottom of the conduction band (X-point) and the top of the valence band (Γ-point), which is typical for semimetals. The small indirect overlap between them leads to the formation of a pseudo band gap with a magnitude of −0.13 eV, in good agreement with other DFT studies [7, 14, 25, 33]. Fig. 2(b) illustrates several important points. First, states below E_{F} are due to Fe d-orbital electrons, whereas states above E_{F} are mainly due to V d-orbital electrons. Secondly, the change of DOS near E_{F} is symmetric, illustrated by the arrows in Fig. 2(b). According to Eqn. 2 this symmetry would also be imposed on the Seebeck coefficient,

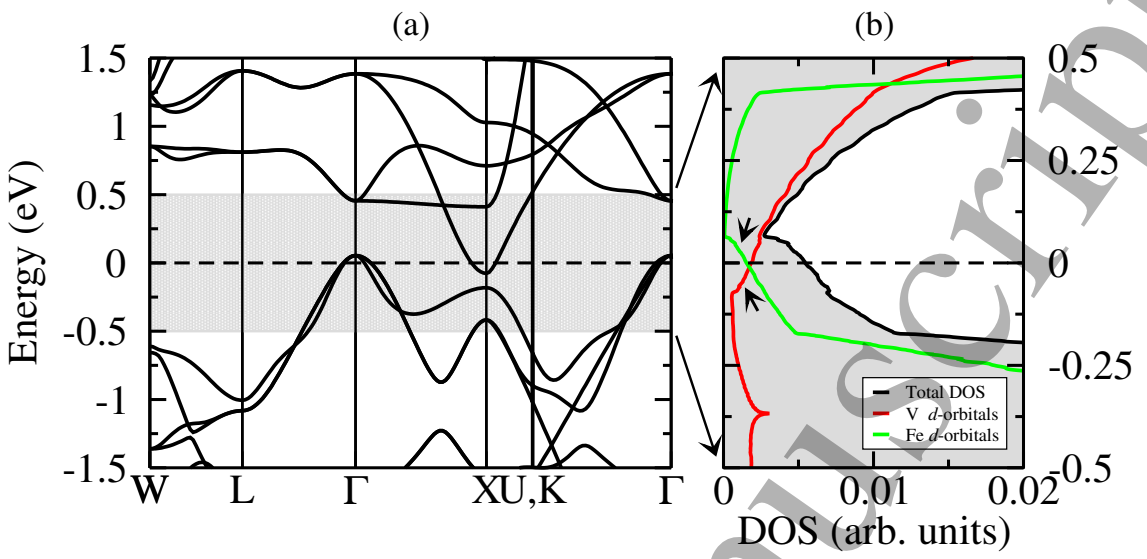

Figure 2. Band structure of Fe_2VAl (a) and the contribution of Fe and V d-orbitals to the total DOS near the Fermi level (b). The small arrows in (b) show the symmetry problem.

consistent with previous theoretical predictions [7]. This predicted symmetry is contrary to the experimentally observed asymmetry of S [6]. Therefore, the similarity in the dispersion of the valence and conduction bands in Fig. 2(a), which is also responsible for the change in DOS near E_F, does not correspond to experimental results [3, 34].

4. The pseudo-gap and the periodicity of the conduction bands

It has been argued in the literature that doping Fe_2VAl changes the position of the pseudo band gap [7, 8]. Next we show that the shift of the pseudo gap is not a result of doping but merely a consequence of the change of the size of the simulation cell. Fig. 3 presents (a) the band structure of the primitive rhombohedral cell along the W-X-L-Γ-X-W path, (b) the band structure obtained with a cubic cell and (c) a $2 \times 2 \times 2$ rhombohedral supercell. The band structure in Fig. 3(b) can be obtained from Fig. 3(a) by folding the right X-point onto the Γ-point and overlaying the X-W section on top of the new Γ-X section. The R-Γ region in Fig. 3(b) can be obtained by folding the W-X-L-Γ section along the L-point towards the Γ-point so that the X-point goes again on top of the Γ-point. The band structure in Fig. 3(c) is obtained by folding the R-Γ section in Fig. 3(b) to the right and overlaying an X-K region from the primitive cell onto the Γ-X region in Fig. 3(c). Therefore, the change in the position of the pseudo band gap is due to band folding rather than doping, and can be seen even in the *undoped* material.

Fig. 3(a) also reveals an interesting periodicity in the conduction bands when plotted along the X-L-Γ-X path. The two X-points are equivalent and form a closed path, but the conduction bands along this path do not return to the same eigenvalues,

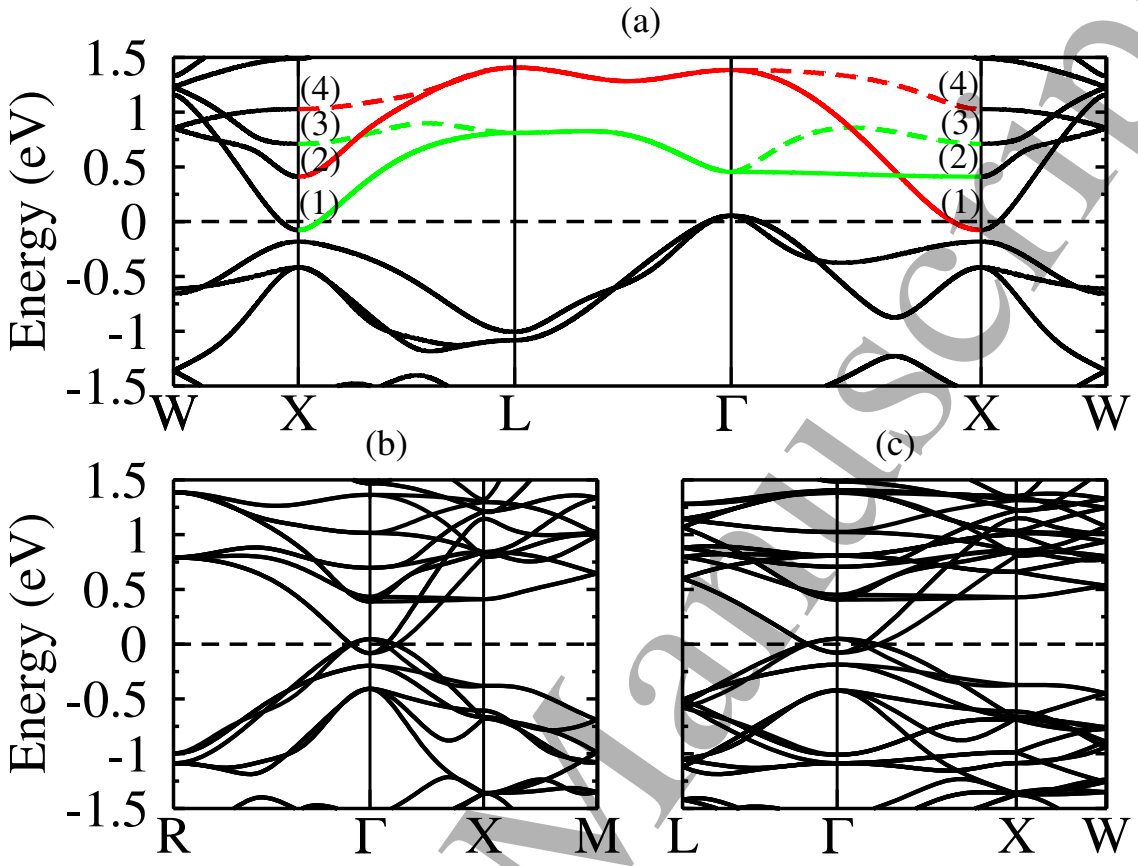

Figure 3. Fe_2VAl band structure of (a) a primitive rhombohedral unit cell; (b) a cubic unit cell; and (c) a $2\times2\times2$ rhombohedral unit cell. The Fermi level is indicated with a horizontal dashed line. The orbital character for each conduction band *exactly* at the X-point in (a) is labelled as (1) V $d_{x^2-y^2}$, (2) Fe $d_{x^2-y^2}$, (3) Fe d_{z^2} and V d_{xz}, (4) Fe d_{z^2}. The green (solid and dashed) bands illustrate the starting (1) and (3) positions at the left X-point and the possible final (2) and (4) positions at the right X-point. The red (solid and dashed) bands illustrate the starting (2) and (4) positions at the left X-point and the possible final (1) and (3) positions at the right X-point.

nor with the same orbital character. This is illustrated by the red and green coloured bands in Fig. 3(a) where at the X-point, the band labelled '1' is due to V and band '2' is due to Fe. Note that the colours of the bands do not represent their orbital character but rather aim to make them distinguishable for the reader and illustrate the changed periodicity. This periodicity is observed with both PBE and LDA exchange-correlation functionals and the only crossing point between the 'red' and 'green' band in Fig. 3(a) happens in a region where there is almost no hybridisation in the bands; this band topology is in agreement with another DFT study [18]. We would further like to emphasise that the PBE band structure is in qualitative disagreement with the experimental evidence (thermoelectric response). It is, of course, perfectly possible for a material to have such features in its band structure, but in this case they arise because of the spurious self-interaction inherent in standard PBE calculations (and LDA) and disappear with even the modest Hubbard U potentials used in this work (see section 5).

Recent ARPES measurements [24] managed to map the top valence bands in Fe_2VAl. Our results agree well with the ARPES mapping and show that these bands are entirely due to Fe. The top valence bands are also responsible for the *p*-type behaviour and magnitude of the Seebeck coefficient, which could be modelled well even within the standard DFT framework. It has also been shown in a recent DFT+DMFT study [35] that the V site displays stronger orbital-localised states than the Fe site. Other theoretical studies, which compute the value of the Hubbard U term, indicate that the U value on Fe should be larger than on V [18]. Nevertheless, the experimental asymmetry of S is not reproduced. Considering all that, we will employ a more pragmatic approach and test different Hubbard U settings in order to model experimental results. In the following sections we apply an additional on-site Coulomb term to V in the form the Hubbard U, while leaving Fe either untouched or with a Hubbard U value smaller than the one used for V.

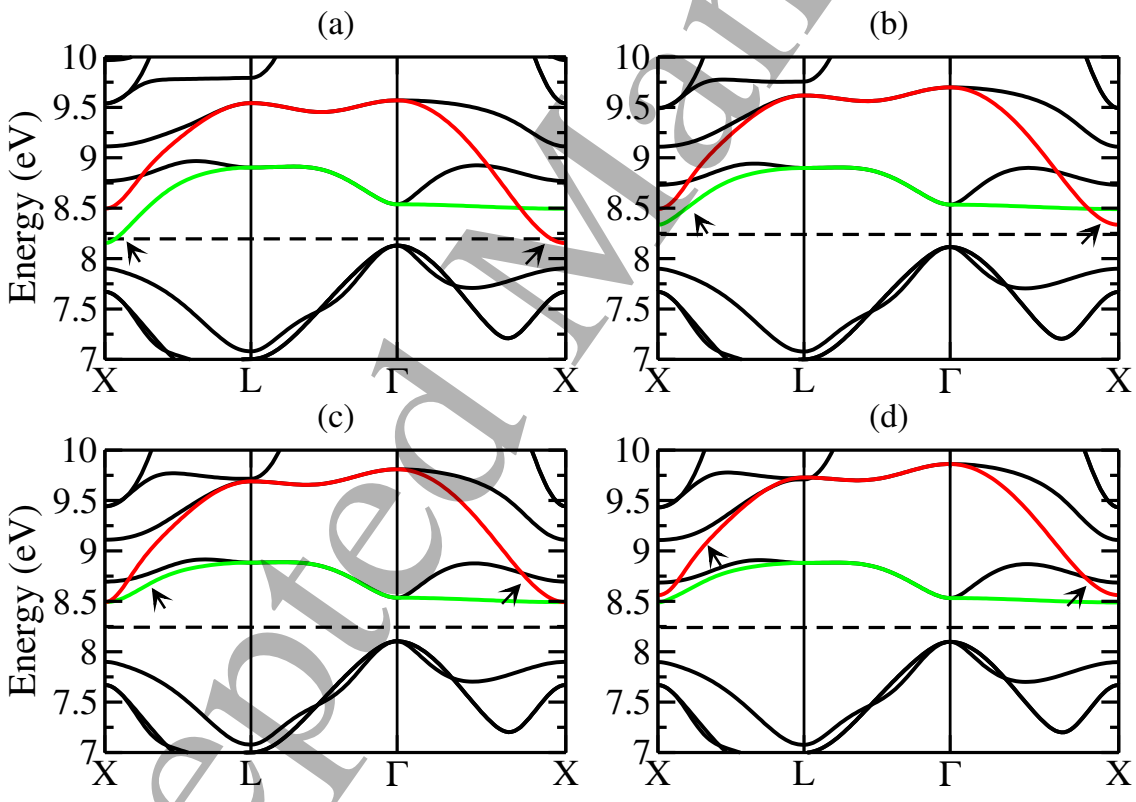

Figure 4. Band structure of Fe_2VAl along the X-L-Γ-X path with U_V of 1.0 eV (a), 2.0 eV (b), 2.75 eV (c) and 3.0 eV (d). The Fermi level is represented by a dashed horizontal line. Arrows indicate which bands are being pushed upwards. The colour of the bands is for illustration purposes and shows that a simple Bloch periodicity is recovered in (c) and (d).

5. Testing the Hubbard model on Fe_2VAl

Next we present the results of the Fe_2VAl band structure initially with the inclusion of the U parameter only on V. Figure 4 shows how the band structure changes when U_V = 1.0, 2.0, 2.75 and 3.0 eV is added (U_{Fe} = 0 eV in all cases). The inclusion of U_V modifies mostly the bottom conduction band at the X-point, as expected and in agreement with another study [18]. The general trend presented in Fig. 4(a)-(d) shows that the eigenvalue of the bottom conduction band at the X-point moves upwards with the increase of U_V. Looking specifically at the X-L section of the band structure, the bottom conduction band (green) moves upwards up to U_V = 2.75 eV. An increase of U_V above 2.75 eV stops affecting the movement of the bottom conduction band (green), while the band above (red) starts moving upwards. As a result, a simple Bloch-style periodicity is recovered for these bands, for all U_V values > 2.75 eV. In addition, the green band in the Γ-X section, which for this region specifically is due to Fe, becomes the major contributor to the conduction states. The flat dispersion of the Fe band in the Γ-X section results in a sharp change in DOS, thus eliminating the symmetry problem outlined in Fig. 2. This result agrees very well with the recent DFT+DMFT study [35] which also reports the lifting of the DFT-based symmetry.

As discussed above we demonstrate that the values of U_V larger than 2.75 eV overcome the DOS symmetry and band structure periodicity issues. The precise value of U_V is difficult to determine without experimental data which maps the dispersion of the V conduction bands in Fe_2VAl, which to the best of our knowledge is not available at present. In order to remain as close as possible to the original PBE exchange-correlation functional the smallest value of U_V (2.75 eV), which solves the problems discussed above, was used for transport properties calculations.

We also compare our results of the band structure with the Hubbard U to the available ARPES data from Soda *et al.* [24] in Fig. 5. There is a set of white bands on top of the ARPES data, which comes from the original study and is also obtained via DFT. For comparison, we added two overlays of our results without the Hubbard U (red overlay) and with the Hubbard U (U_V =2.75 eV; green overlay). In both cases, the bands responsible for the p-type Seebeck coefficient maximum (between 0 and -1 eV) overlap with the results of the ARPES study.

The inclusion of the Hubbard U only on V opens a modest band gap of 0.4 eV. This value of the band gap results in an overestimate of S maxima when compared to the experimental results [3]. As indicated by the more accurate DFT+DMFT method [35] the band gap is a lot smaller at low temperatures. Therefore, a scissors operator was added to the thermoelectric calculations in order to correct for the significant increase in S. The scissors operator set the difference between the top conduction and valence bands to 0.04 eV and 0.2 eV at the Γ- and X-points, respectively, with an overall (indirect) band gap value of 0 eV. This zero-band gap semiconductor model is also implied by experimental studies [34].

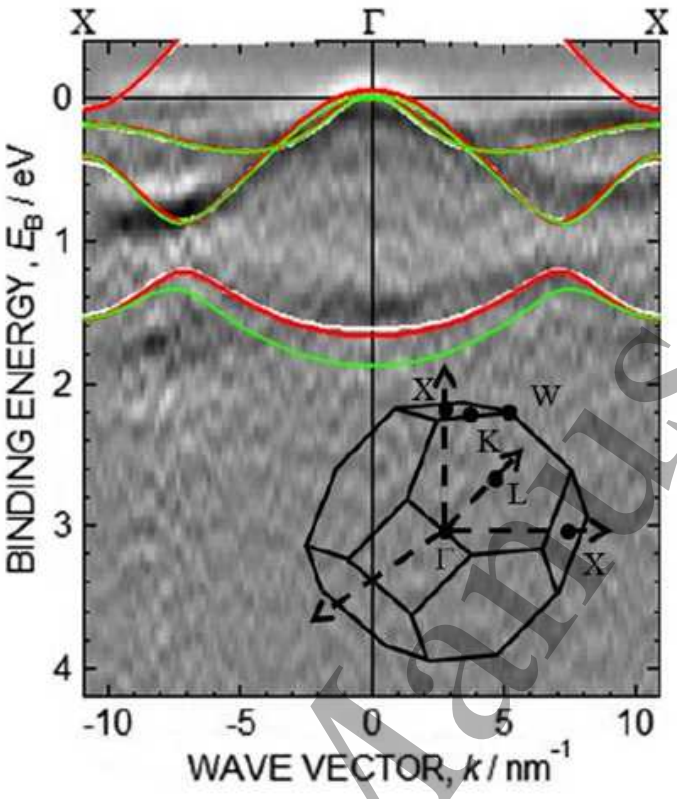

Figure 5. Comparison between Soda *et al.* [24] experimental (ARPES; grey backgrounds) and theoretical results (white bands) and band structures obtained in this study without the Hubbard U (red bands) and with the Hubbard U (U_V =2.75 eV; green bands).

6. Electronic thermoelectric properties

Considering the Hubbard U on V and the scissors operator correction we calculated the thermoelectric properties of Fe_2VAl at room temperature. The calculated values of S, σ/τ and $\kappa_{el}\tau$ within PBE and PBE + Δ, with $\Delta = U$ + scissors operator, are presented in Fig. 6. The Seebeck coefficient maxima obtained within PBE (Fig. 6(a), black line) are 58 and -52 μV/K for p- and n-type, respectively. This is in good agreement with other theoretical studies [7, 16, 18, 36], but as expected disagrees with experimental results [6, 34]. In contrast, the maximum values of S obtained within PBE + Δ (Fig. 6(a), green line) yield 76 and -158 μV/K for p- and n-type, respectively. These results capture the asymmetry in the variation of S and are now in good agreement with the experimental results [3, 2]. The values of σ/τ and κ_{el}/τ (Fig. 6(b) and (c)) within the constant relaxation time approximation are presented in Table 1. The value of τ (Table 1) is obtained by fitting the theoretical value of $1/\sigma$ to the experimental one of 0.75 mΩcm [34, 37].

Our calculations also showed that the theoretically obtained maxima of S heavily depend on the strength of the scissors operator, in agreement with other studies [16,

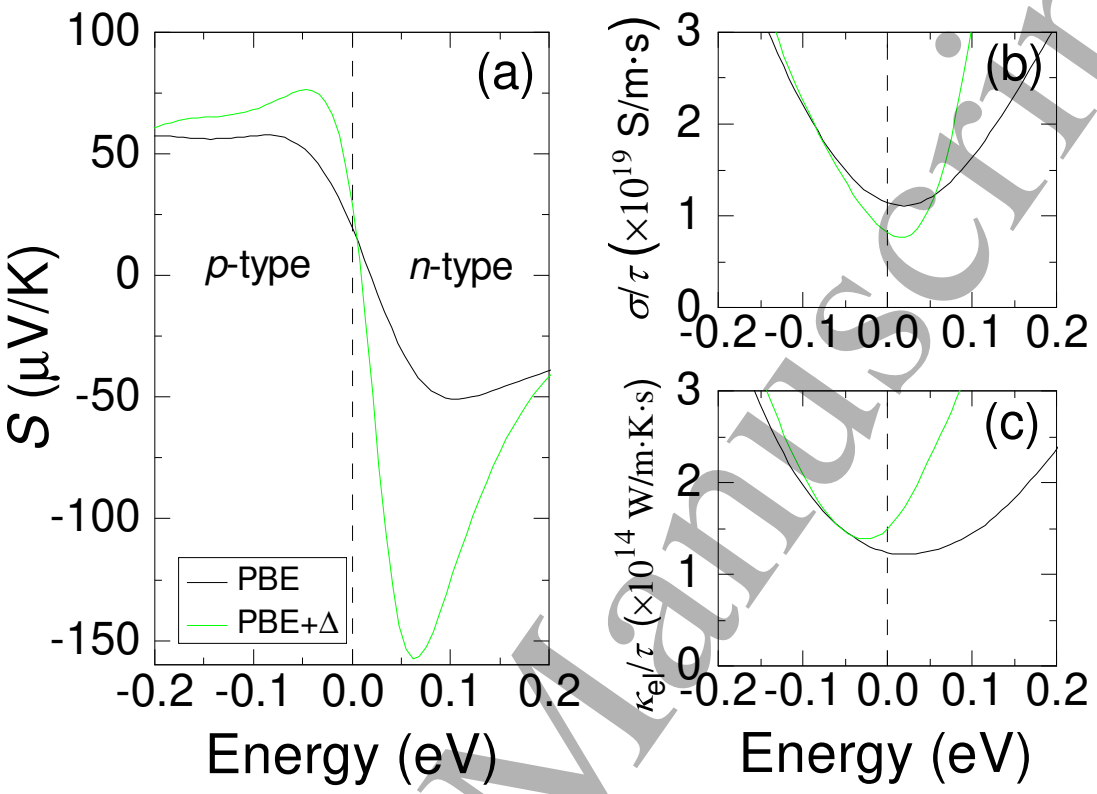

Figure 6. Thermoelectric properties of Fe_2VAl at T=300 K. Black and green solid lines represent results obtained within PBE and PBE + Δ, respectively; Δ represents U + scissors operator. Fermi level is indicated by a vertical dashed line at 0 eV. The subfigures show the Seebeck coefficient (a), electrical conductivity (b) and the electronic thermal conductivity (c).

Table 1. Values of σ/τ, κ_{el}/τ and τ obtained within PBE and PBE + Δ.

Method	σ/τ ($\Omega^{-1}m^{-1}s^{-1}$)	$\kappa_{el/\tau}$ ($Wm^{-1}K^{-1}s^{-1}$)	τ (s)
PBE	1.14×10^{19}	1.23×10^{14}	1.17×10^{-14}
PBE + Δ	0.82×10^{19}	1.50×10^{14}	1.62×10^{-14}

18, 17]. A small variation of 30 meV in the magnitude of the band gap (set at 0 eV in the present calculations) moves the maximum of S across the whole experimental range, especially for the n-type semiconductor. Therefore, the uncertainty in the experimental [2, 3, 6] measurements of S makes it difficult to determine the precise value of the band gap. Furthermore, we also note that the valence bands at the X-point (Fig. 4(d)) are slightly lower in energy compared to ARPES measurements [24]. As shown in this study, the bands dispersion determines the magnitude and the symmetry of the Seebeck coefficient. Therefore, a small increase in the energy of the bands at the X-point would increase the p-type and decrease the n-type values of S, putting them in even better agreement with experimental data.

(a)

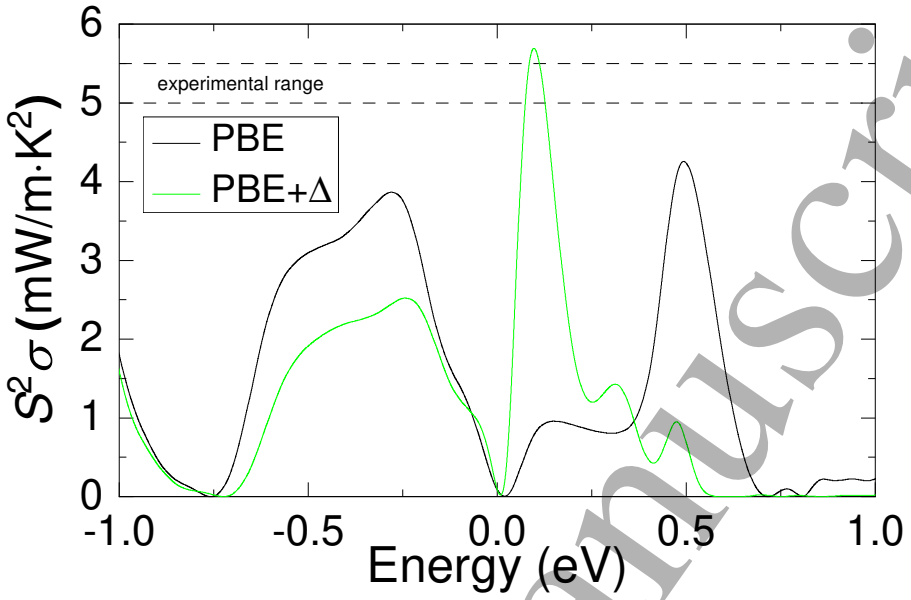

(b)

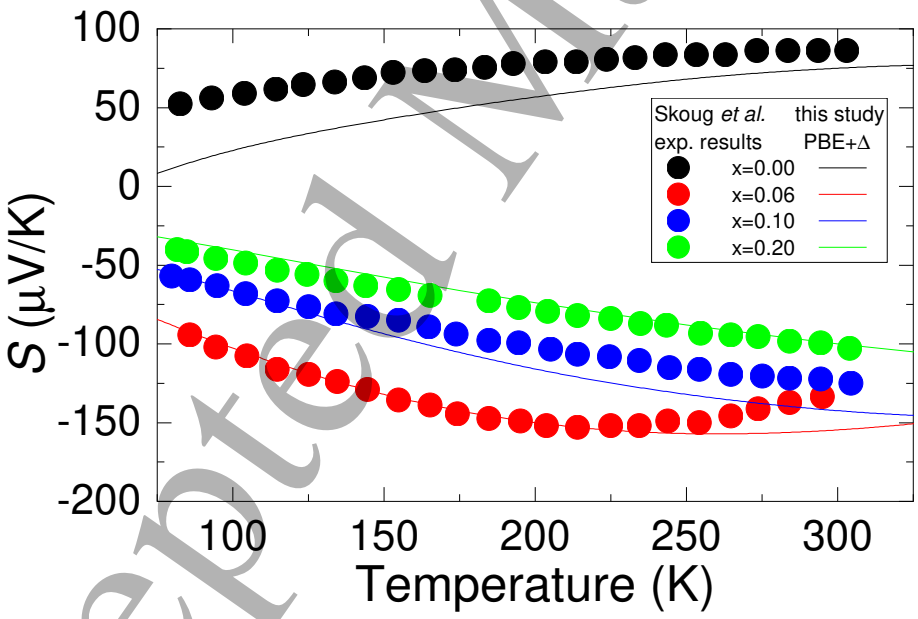

Figure 7. Power factor (a) of Fe_2VAl at T=300 K for PBE (black) and PBE + Δ (green); Δ represents U + scissors operator. Horizontal dashed lines show the experimental range for the power factor. Comparing S (b) obtained with PBE + Δ and experimental measurements at different doping levels [2]. Doping values of x are with an included offset of 0.027 to the p-type side to take into account the intrinsic number of holes in experimental samples. This value is obtained by using the experimentally reported S for bulk Fe_2VAl at 300 K as a reference point.

Next we show a further comparison between our theoretical prediction and experimental results in Fig. 7. Subfigure (a) shows the power factor computed with PBE

(black) and PBE + Δ (green). We compare *n*-type *PF* performance to the reported experimental values (horizontal dashed lines) between 5.0–5.5 mW/m·K^2 [38, 2] for $Fe_2VAl_{1-x}Si_x$ with $x = 0.1$. We obtain a new value for τ by fitting the theoretical value of $1/\sigma$ to the experimental one of 0.35 mΩcm for $x = 0.1$ in $Fe_2VAl_{1-x}Si_x$ [2]. Chemical doping of x=0.01 corresponds to an energy of 0.09 eV above the Fermi level in the PBE + Δ model in Fig. 6. Compared to τ values in Table 1 the relaxation time increases by 65% for PBE and decreases by 27% for PBE + Δ. A reduction in τ is the expected behaviour as dopants increase the scattering rates. Regarding the power factor we see that the *n*-type peak for the PBE + Δ curve agrees very well with experimental results and falls within the experimental range marked by the horizontal dashed lines. In addition, the BoltzTraP analysis shows that the position of the peak for the PBE + Δ curve matches the expected experimental doping level of x=0.1, whereas the position of peak obtained without the Hubbard U (black curve around 0.5 eV) suggests an unrealistically high doping of x=0.35. Figure 7(b) compares the Seebeck coefficient obtained via PBE + Δ to experimental results for doping concentrations of 0, 6, 10 and 20% additional electrons per formula unit [2]. The good agreement between our prediction and experimental measurements means that the PBE + Δ method not only captures correctly the maximum values of the Seebeck peaks for *p*- and *n*-type semiconductor but also model properly their position and spread along the chemical potential.

7. Applying the Hubbard model to Fe and V

We know from other studies [18] that having a larger Hubbard U on Fe than V does not result in an asymmetric S. Based on our calculations we find that the U value on V needs to be at least 2.75 eV in order to make the conduction bands periodic and recreate the asymmetry in S. In principle, this suggests that the Hubbard U on V needs to be 2.75 eV higher than the U on Fe but does not indicate what would happen if $U_{\mathrm{Fe}} > 0$. As we are using a very pragmatic approach to the problem we would like to investigate if the difference of 2.75 eV remains the same when we apply the Hubbard U model to both V and Fe with $U_{\mathrm{V}} > U_{\mathrm{Fe}}$.

Figure 8 shows the Seebeck coefficient when there is a Hubbard U on both V and Fe, with $U_{\mathrm{V}} > U_{\mathrm{Fe}}$. We have set the band gap to 0 eV for all cases when it had a positive value. Results are presented with dotted and solid curves. Dotted curves do not exhibit the expected asymmetry of S. We note that in all dotted cases bottom conduction bands exhibited the periodicity problem. In contrast, solid curves all agree with each other and recreate the asymmetric behaviour of S, similarly to the result shown in Fig. 6(a). In addition to our initial settings of $U_{\mathrm{Fe}} = 0$ eV and $U_{\mathrm{V}} = 2.75$ eV (green curve), other successful attempts included $U_{\mathrm{Fe}} = 1$ eV and $U_{\mathrm{V}} = 3.2$ eV (red curve), and $U_{\mathrm{Fe}} = 2$ eV and $U_{\mathrm{V}} = 4$ eV (blue curve). The difference between U_{Fe} and U_{V} gradually falls down to 2 eV when we add the Hubbard U to the Fe atoms. We noted that all solid curve examples belong to cases in which the lowest conduction bands are periodic. Based

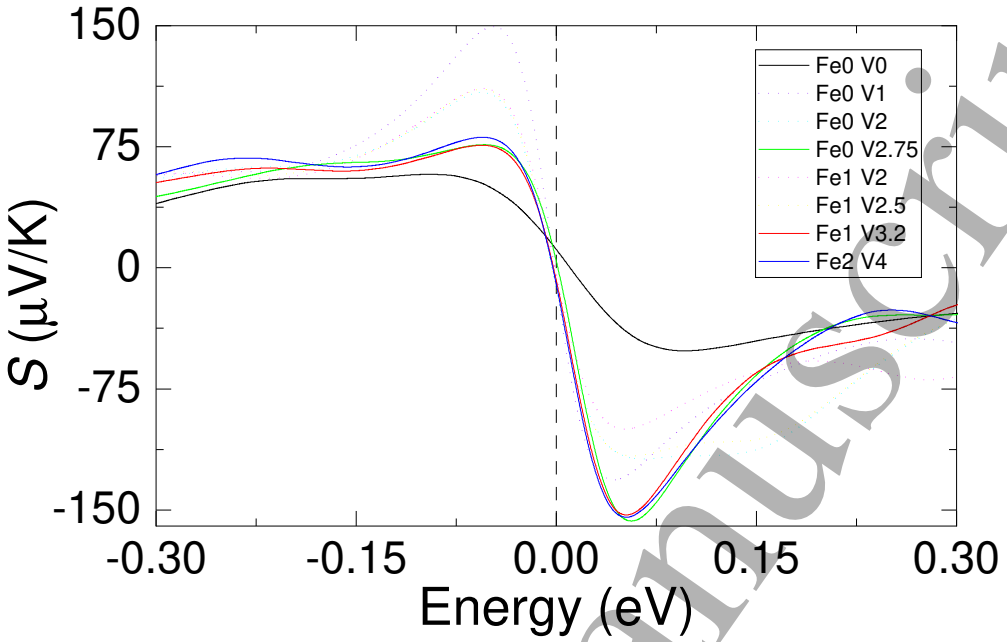

Figure 8. Comparing how different Hubbard U settings on Fe and V affect S of Fe_2VAl at T=300 K. Solid curves show cases when conduction bands are periodic. Dotted curves represent cases when conduction bands are non periodic.

on Fig. 8 results we can conclude that even with $U_{\mathrm{Fe}} > 0$ eV, the Seebeck coefficient of Fe_2VAl can exhibit the expected experimental asymmetric behaviour as long as the localisation on V atoms is stronger and the conduction bands are periodic.

One might wonder whether the PBE + Δ approach would remain applicable for more challenging structures where no experimental data is available. For simple doping, e.g. with Si or Ge, the states around E_{F} remain unaffected and the parameters used in this study will be the same. For off-stoichiometric compounds, it was shown experimentally by Nishino and Tamada [3] that the asymmetry in S is always present. As our method does not affect the valence states in Fe_2VAl, the magnitude of the p-type peak of S could be used as a guide to deduce the value of the scissors operator for more complicated structures. Alternatively, if the power factor is used as a reference point, then the scissor operator becomes less significant since for any positive value of the band gap, changes in S and σ compensate each other and yield no net change in the power factor. In most cases, the aim of more challenging modifications of Fe_2VAl is to reduce the lattice thermal conductivity, and our approach provides a very cheap way of checking whether the rest of the thermoelectric properties are affected. Our method makes it obvious that Fe_2VAl is a special compound which is hard to model within the conventional DFT/DFT+U framework. Analysis of the results should be done with care and for more challenging structures it would be appropriate to check the accuracy of the results with a higher level of theory, e.g. the more expensive but more accurate DFT+DMFT method.

8. Conclusions

In summary, our calculations show that in simple DFT the lowest conduction bands in Fe_2VAl have different periodicity to the valence bands. The inclusion of $U_V > 2.75$ eV modifies the bands' dispersion, recovering a Bloch-periodicity, and changes the order of the lowest conduction bands from V to Fe being at the bottom. As a result, the experimentally observed asymmetry in S can be theoretically reproduced. Furthermore, Fe_2VAl was modelled as a zero-band gap semiconductor by adding a scissors operator to the transport calculations. Thus, the maxima of S become $+76$ and -158 μV/K for p- and n-type, respectively, in good agreement with experimental results [3]. The ability of our approach to model simultaneously the p- and n-type sides around E_F provides a good starting point for understanding the thermoelectric properties of Fe_2VAl, as well as further studies which may include structure modifications or movement along the chemical potential in pursuit of a better thermoelectric figure of merit (ZT). We note that this should be accompanied by a very careful interpretation and analysis of the results, especially for more challenging structures.

Acknowledgements

PJH acknowledges financial support from EPSRC (grant ref. EP/R025770/1). We are grateful for computational support from the UK national high performance computing service, ARCHER, for which access was obtained via the UKCP consortium and funded by EPSRC grant ref. EP/P022561/1.

References

[1] Y Nishino, M Kato, S Asano, K Soda, M Hayasaki, and U Mizutani. Semiconductorlike Behavior of Electrical Resistivity in Heusler-type Fe_2VAl Compound. *Physical Review Letters*, 79(10):1909–1912, September 1997.

[2] Eric J Skoug, Chen Zhou, Yanzhong Pei, and Donald T Morelli. High Thermoelectric Power Factor Near Room Temperature in Full-Heusler Alloys. *Journal of Electronic Materials*, 38(7):1221–1223, July 2009.

[3] Y Nishino and Y Tamada. Doping effects on thermoelectric properties of the off-stoichiometric Heusler compounds $Fe_{2-x}V_{1+x}Al$. *Journal of Applied Physics*, 115(12):123707, March 2014.

[4] Hidetoshi Miyazaki, Manabu Inukai, and Yoichi Nishino. Effect of Ta substitution on the electronic structure of Heusler-type Fe_2VAl-based alloy. *Journal of Applied Physics*, 120(12):125106, September 2016.

[5] M Vasundhara, V Srinivas, and V V Rao. Low-temperature electrical transport in Heusler-type $Fe_2V(AlSi)$ alloys. *Journal of Physics: Condensed Matter*, 17(38):6025–6036, September 2005.

[6] Y Nishino. Development of thermoelectric materials based on Fe_2VAl Heusler compound for energy harvesting applications. *IOP Conference Series: Materials Science and Engineering*, 18(14):142001, May 2011.

[7] H Al-Yamani and B Hamad. Thermoelectric Properties of Fe_2VAl and $Fe_2V_{0.75}M_{0.25}Al$ (M = Mo, Nb, Ta) Alloys: First-Principles Calculations. *Journal of Electronic Materials*, 45(2):1101–1114, February 2016.

[8] Ch Venkatesh, S K Srivastava, and V V Rao. First principle investigations on boron doped Fe_2VAl Heusler alloy. *Physica B: Condensed Matter*, 448:237–243, September 2014.

[9] M Mikami, M Inukai, H Miyazaki, and Y Nishino. Effect of Off-Stoichiometry on the Thermoelectric Properties of Heusler-Type Fe_2VAl Sintered Alloys. *Journal of Electronic Materials*, 45(3):1284–1289, March 2016.

[10] Sébastien Lemal, Fabio Ricci, Daniel I Bilc, Matthieu J Verstraete, and Philippe Ghosez. Magnetic instabilities in doped Fe_2YZ full-Heusler thermoelectric compounds. *Physical review. B, Condensed matter*, 100(16):161201, October 2019.

[11] K Kudo, S Yamada, J Chikada, Y Shimanuki, T Ishibe, S Abo, H Miyazaki, Y Nishino, Y Nakamura, and K Hamaya. Significant reduction in the thermal conductivity of Si-substituted Fe_2VAl epilayers. *Physical review. B, Condensed matter*, 99(5):054201, February 2019.

[12] Subrahmanyam Bandaru, Ankita Katre, Jesús Carrete, Natalio Mingo, and Philippe Jund. Influence of Antisite Defects on the Thermoelectric Properties of Fe_2VAl. *Nanoscale and Microscale Thermophysical Engineering*, pages 1–10, July 2017.

[13] Georg K H Madsen and David J Singh. BoltzTraP. A code for calculating band-structure dependent quantities. *Computer Physics Communications*, 175(1):67–71, July 2006.

[14] G Y Guo, G A Botton, and Y Nishino. Electronic structure of possible 3d 'heavy-fermion' compound. *Journal of Physics: Condensed Matter*, 10(8):L119, January 1999.

[15] D J Singh and I I Mazin. Electronic structure, local moments, and transport in Fe_2VAl. *Physical Review B*, 57(22):14352–14356, June 1998.

[16] Daniel I Bilc and Philippe Ghosez. Electronic and thermoelectric properties of Fe_2VAl: The role of defects and disorder. *Physical Review B*, 83(20):1–4, May 2011.

[17] Shamim Sk and Sudhir K Pandey. Studying the Seebeck coefficient of Fe2VAl compound in the high temperature region. *AIP conference proceedings*, 2115(1):030424, July 2019.

[18] Dat Do, Mal-Soon Lee, and S D Mahanti. Effect of onsite Coulomb repulsion on thermoelectric properties of full-Heusler compounds with pseudogaps. *Physical Review B*, 84(12):125104, September 2011.

[19] A Bansil, S Kaprzyk, P E Mijnarends, and J Toboła. Electronic structure and magnetism of $Fe_{3-x}V_xX$ (X = Si , Ga, and Al) alloys by the KKR-CPA method. *Physical Review B*, 60(19):13396–13412, November 1999.

[20] M Weinert and R E Watson. Hybridization-induced band gaps in transition-metal aluminides. *Physical Review B*, 58(15):9732–9740, October 1998.

[21] K Soda, H Murayama, K Shimba, S Yagi, J Yuhara, T Takeuchi, U Mizutani, H Sumi, M Kato, H Kato, Y Nishino, A Sekiyama, S Suga, T Matsushita, and Y Saitoh. High-resolution soft x-ray photoelectron study of density of states and thermoelectric properties of the Heusler-type alloys $(Fe_{2/3}V_{1/3})_{100-y}Al_y$. *Physical Review B*, 71(24):245112, June 2005.

[22] H Okamura, J Kawahara, T Nanba, S Kimura, K Soda, U Mizutani, Y Nishino, M Kato, I Shimoyama, I, H Miura, K Fukui, K Nakagawa, H Nakagawa, and T Kinoshita. Pseudogap formation in the intermetallic compounds $(Fe_{1-x}V_x)_3Al$. *Physical Review Letters*, 84(16):3674–3677, April 2000.

[23] M Kato, Y Nishino, S Asano, and S Ohara. Electrical resistance anomaly and Hall effect in $(Fe_{1-x}V_x)_3Al$ alloys. *Journal of the Japan Institute of Metals*, 62(7):669–674, March 1998.

[24] K Soda, S Harada, T Hayashi, M Kato, F Ishikawa, Y Yamada, S Fujimori, and Y Saiyoh. Angle-Resolved Photoemission Analysis of Electronic Structures for Thermoelectric Properties of Off-Stoichiometric $Fe_{2-x}V_{1+x}Al$ Alloys. *Materials Transactions*, 57(7):1040–1044, April 2016.

[25] Manish Kumar, Tashi Nautiyal, and Sushil Auluck. First-principles calculations of electronic and optical properties of $Fe_{3-x}V_xAl$ (x=0–3) compounds. *Journal of Physics: Condensed Matter*, 21(44):446001, November 2009.

[26] E Shreder, S Streltsov, A Svyazhin, A Lukoyanov, and V Anisimov. Electronic structure and physical properties of Fe_2MAl (M = Ti ,V ,Cr) Heusler alloys. In *Proceedings of the Third Moscow International Symposium on Magnetism*, pages 7–10, June 2005.

[27] Stewart J Clark, Matthew D Segall, Chris J Pickard, Phil J Hasnip, Matt I J Probert, Keith Refson, and Mike C Payne. First principles methods using CASTEP. *Zeitschrift für Kristallographie - Crystalline Materials*, 220(5/6):567–570, January 2005.

[28] J P Perdew, K Burke, and M Ernzerhof. Generalized Gradient Approximation Made Simple. *Physical Review Letters*, 77(18):3865–3868, October 1996.

[29] Hendrik J Monkhorst and James D Pack. Special points for Brillouin-zone integrations. *Physical Review B*, 13(12):5188–5192, June 1976.

[30] Andrew J Morris, Rebecca J Nicholls, Chris J Pickard, and Jonathan R Yates. OptaDOS: A tool for obtaining density of states, core-level and optical spectra from electronic structure codes. *Computer Physics Communications*, 185(5):1477–1485, May 2014.

[31] Sir Nevill Francis Mott and H Jones. *The Theory of the Properties of Metals and Alloys*. Courier Corporation, January 1958.

[32] I Galanakis, Ph Mavropoulos, and P H Dederichs. Electronic structure and Slater–Pauling behaviour in half-metallic Heusler alloys calculated from first principles. *Journal of Physics D: Applied Physics*, 39(5):765, February 2006.

[33] Ruben Weht and W E Pickett. Excitonic correlations in the intermetallic Fe_2VAl. *Physical Review B*, 58(11):6855–6861, September 1998.

[34] M Vasundhara, V Srinivas, and V Rao. Electronic transport in Heusler-type $Fe_2VAl_{1-x}M_x$ alloys (M = B, In, Si). *Physical Review B*, 77(22):224415, June 2008.

[35] Oleg Kristanovski, Raphael Richter, Igor Krivenko, Alexander I Lichtenstein, and Frank Lechermann. Quantum many-body intermetallics: Phase stability of Fe_3Al and small-gap formation in Fe_2VAl. *Physical Review B*, 95(4):045114, January 2017.

[36] Bin Xu, Yuanxu Wang, Wenjie Zhao, and Yuli Yan. Thermoelectric properties of Heusler-type compound $Fe_2V_{1-x}Nb_xAl$. *Journal of Applied Physics*, 110(1):013530, July 2011.

[37] Y Nishino, S Deguchi, and U Mizutani. Thermal and transport properties of the Heusler-type $Fe_2VAl_{1-x}Ge_x$ ($0 \leq x \leq 0.20$) alloys: Effect of doping on lattice thermal conductivity, electrical resistivity, and Seebeck coefficient. *Physical Review B*, 74(11):1–6, September 2006.

[38] Hideaki Kato, Masaaki Kato, Yoichi Nishino, Uichiro Mizutani, and Shigeru Asano. Effect of Silicon Substitution on Thermoelectric Properties of Heusler-type Fe_2VAl Alloy. *Journal of the Japan Institute of Metals*, 65(7):652–656, May 2001.